RSC Advances

PAPER

View Article Online
View Journal | View Issue

Cite this: *RSC Adv.*, 2016, **6**, 84926

Explaining RANKL inhibition by OPG through quantum biochemistry computations and insights into peptide-design for the treatment of osteoporosis†

Bruno L. Sousa,*[a] Ito L. Barroso-Neto,[b] Evanildo F. Oliveira,[a] Emerson Fonseca,[c] Pedro Lima-Neto,[b] Luiz O. Ladeira[c] and Valder N. Freire[a]

Received 29th June 2016
Accepted 21st August 2016

DOI: 10.1039/c6ra16712h

www.rsc.org/advances

Osteoporosis is a degenerative disease associated with excessive bone resorption, a natural process performed by osteoclasts. In turn, osteoclast maturation is critically regulated by the receptor activator of nuclear factor kB ligand (RANKL), its signalling receptor (RANK), and its decoy receptor osteoprotegerin (OPG). The critical role of the protein triad, RANK–RANKL–OPG, in osteoclastogenesis has made their binding an important target for the rational development of drugs against osteoporosis. Based on this, we have performed a quantum biochemistry investigation of the binding between RANKL and its decoy receptor, OPG, in order to analyse the individual contributions of all amino acid residues involved in the complex formation, providing a deeper understanding of the inhibition process. The role of specific residues in the RANKL–OPG binding was evaluated through quantum biochemistry computations performed within the molecular fractionation with conjugate caps (MFCC) methodology, and inter-residue binding energies were calculated within the framework of density functional theory (DFT). Our simulations, considering water effects (implicit and explicit) and the role of the dielectric constant background, attested the major importance of site II, when compared to site I, over OPG binding and functionality, mainly through interactions performed by the tripeptide OPG core, I94–E95–F96. The obtained results also explain (i) the impact of a specific OPG mutation (F96L) on Paget's disease development; (ii) how some pioneers proposed that peptides efficiently inhibit the RANKL–OPG complex, acting as promising drugs for the treatment of osteoporosis. In conclusion, our quantum biochemistry approach provides a solid base that allows important insights into peptide and drug design for the treatment of osteoporosis based on RANKL–OPG binding inhibition.

1. Introduction

The processes of bone formation and resorption mediate an essential equilibrium for bone health, known as bone remodelling, which is regulated by osteoblasts and osteoclasts, respectively.[1–3] Osteoclasts are multinucleated bone resorbing cells formed by cytoplasmic fusion of mononuclear precursors, which are in the myeloid lineage of hematopoietic cells that also give rise to macrophages.[4] The osteoclast maturation process is critically regulated by a protein triad composed of the receptor activator of nuclear factor kB ligand (RANKL), its signalling receptor (RANK), and its decoy receptor, osteoprotegerin (OPG).[3,5]

RANKL is a member of the tumor necrosis factor (TNF) superfamily, expressed as a homotrimeric transmembrane or secreted protein in osteoblasts, which plays a central role in osteoclast formation and bone resorption.[6–8] The binding of RANKL to RANK, present at the membrane of osteoclast precursors, leads to the trimerization of this receptor and promotes osteoclast differentiation and activation through a downstream signalling cascade.[9] On the other hand, OPG is secreted by osteoblasts and inhibits the binding of RANKL to RANK, thereby limiting osteoclastogenesis.[9] OPG occurs as a dimer and can act as a decoy receptor of RANKL in view of structural similarities to the RANK ectodomain.[10] Recently, it has been reported that the leucine-rich repeat-containing G-protein-coupled receptor 4 (LGR4) is another receptor for RANKL, inhibiting osteoclastogenesis through competition with RANK and by downstream signalling. However, the soluble version of this protein (LGR4-ECD) presented lower binding

[a]*Departamento de Física, Universidade Federal do Ceará, 60455-760, Fortaleza, Ceará, Brazil. E-mail: brunolopesdesousa@gmail.com*

[b]*Departamento de Química Analítica e Físico-Química, Universidade Federal do Ceará, 60455-760, Fortaleza, Ceará, Brazil*

[c]*Departamento de Física, Universidade Federal de Minas Gerais, Belo Horizonte, Minas Gerais, Brazil*

† Electronic supplementary information (ESI) available. See DOI: 10.1039/c6ra16712h

affinity than OPG for RANKL, and had little physiological effect on osteoclast differentiation.[11]

Bone remodelling becomes perturbed in a variety of pathological conditions that affect the skeleton, including postmenopausal osteoporosis and rheumatoid arthritis,[12] in which there is local and/or systemic alteration in the levels of hormones or proinflammatory cytokines that are known to stimulate or inhibit bone resorption *in vitro* and *in vivo*.[4] Functional mutations in RANKL lead to human autosomal recessive osteopetrosis (ARO), whereas RANKL overexpression has been implicated in the pathogenesis of bone degenerative diseases, such as osteoporosis, demonstrating that RANKL and RANK are indispensable for osteoclastogenesis, whereas the absence of OPG causes increased osteoclastogenesis and osteopenia.[13] Although RANKL is best known for its role in bone resorption, it also plays multiple roles in the immune system,[6,7,14–18] mammary gland development during pregnancy,[19] thermoregulation,[20] heart diseases,[21] cancer metastasis,[22,23] and hormone-derived breast development.[24] Therefore, the RANK–RANKL–OPG molecular triad is an attractive target for the development of rational therapies to prevent bone destruction in many osteopenic conditions, such as osteoporosis and arthritis.[10,25]

Among the currently available agents to prevent or treat bone loss, we can mention estrogen, calcitonin and bisphosphonates.[26] Estrogen plays a key role in regulating bone loss and it has been used for the treatment of postmenopausal women, reducing the percentage of RANKL-expressing cells, but it remains unclear if this is a direct or indirect effect of estrogen.[27] On the other hand, calcitonin has proven efficiency in inhibiting osteoclastogenesis, but it is frequently associated with side effects, such as nausea and flushing.[28] In clinical trials, bisphosphonates are widely used as therapeutic agents, but they may cause some adverse gastrointestinal effects, such as osteonecrosis of the jaw, and renal toxicity.[29]

Alternative therapies based on the development of specific antibodies for the RANK–RANKL–OPG molecular triad are currently under development. The first RANKL inhibitor approved for the treatment of osteoporosis and the prevention of skeleton-related events, named denosumab, consists of a fully human monoclonal antibody against RANKL, which binds to a specific loop region (DE loop) on the ligand and prevents its binding to RANK on responding cells, avoiding osteoclast maturation.[5,30] However, the use of macromolecules, such as antibodies and cytokines, for therapeutics is associated with many disadvantages, such as poor bioavailability, neutralizing antibody production, rebound symptoms, limited long term efficiency, low stability, and a risk of severe and sometimes life-compromising side effects resulting from the antigen–antibody reaction.[31] Additionally, they are costly and there are insurance issues stemming from their high expense.[32,33] Recently, it has been reported that the leucine-rich repeat-containing G-protein-coupled receptor 4 (LGR4) is another receptor for RANKL, inhibiting osteoclastogenesis through competition with RANK and by downstream signalling, but the soluble version of this protein (LGR4-ECD) presented lower binding affinity than OPG for RANKL and had little physiological effect on osteoclast differentiation.[11] A different strategy is exemplified by the use of a truncated version of the human parathyroid hormone (PTH) as a therapeutic for the treatment of osteoporosis.[34] The recombinant version of this long peptide (34 residues), named teriparatide (Forteo®), increases bone remodelling, formation, and density, improves bone microstructure and reduces fracture risk.[35] Nevertheless, this therapeutic presented a high incidence of osteosarcomas, documented in preclinical animal models, with a few cases confirmed for humans.[36]

In the current scenario, the design of biocompatible inhibitory peptides targeting specific protein–protein interactions (PPIs) is available as an interesting alternative approach for the treatment of different pathological conditions, since these interactions are involved in most cellular processes and influence biological functions through proximity-induced changes in protein features.[37–40] Additionally, peptide-based therapeutics are attractive in view of their high biological activity, associated with low toxicity and high specificity, including benefits such as specific binding, minimization of undesired interactions between drugs and reduced tissue accumulation, decreasing risks of complications due to intermediate metabolites.[41] Based on this, the modulation of PPIs is considered a promising strategy towards next-generation therapeutics.[37]

Peptides are unique candidates for rational drug development, since they are flexible in adopting and mimicking local structural features of proteins, being generally non-immunogenic in view of their low molecular weight.[42] In contrast to small molecular ligands that bind to defined protein pockets, the interfaces of PPIs often involve rather flat protein surfaces that exhibit large contact areas. The classical structure-based method for designing therapeutic peptides takes advantage of the amino acid sequences found at PPI sites, which can occur between two structured protein domains, a structured domain and a relatively short peptide, or between two peptide stretches. In many cases, additional weak contacts distant to the defined interaction area contribute to binding, complicating the prediction of PPI characteristics.[43] However, the analysis of several PPI interfaces revealed that specific residue side chains mainly contribute to the Gibbs energy of protein–protein binding. These so-called hot-spot residues often overlap with structurally conserved regions and represent a common feature of PPI interfaces.[44,45]

The molecular structure of murine RANKL has been available for a long time, and recently the molecular structures for murine RANK–RANKL and human RANKL–OPG complexes, as well as the hybrid complex between murine RANK and human RANKL, have also been determined, providing important details related to ligand/receptor interactions in the RANK–RANKL–OPG molecular triad.[10,46,47] RANKL interacts with OPG through three distinct but equivalent shallow grooves located between monomers in the trimer (Fig. 1). Biochemical studies have indicated a ratio of 1 : 1 in the trimer/dimer RANKL–OPG complex, where OPG monomers both bind to the same RANKL trimer, and each monomer of OPG cannot bind to a separate RANKL trimer.[48] This allows efficient inhibition of RANKL-induced RANK trimerization, which is essential for subsequent signalling and osteoclast maturation.

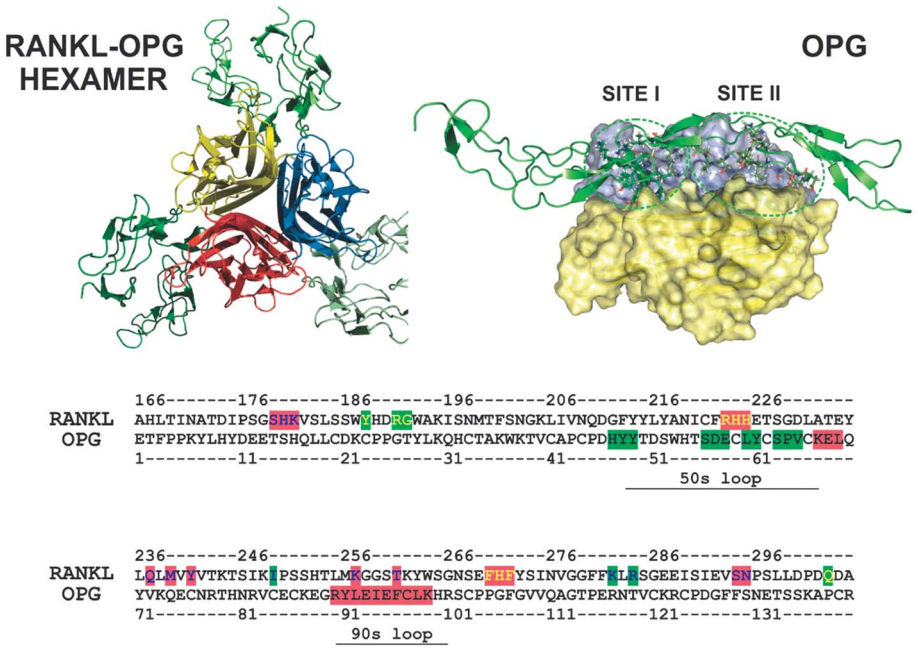

Fig. 1 RANKL–OPG assembly. The left panel presents the hexamer composed of one RANKL trimer bound to three OPG units, obtained from crystallographic data. The RANKL–OPG interface located between two RANKL units and composed of two distinct anchorage sites is presented in the right panel. A sequence representation of all the amino acid paths involved in the interface is shown in the lower panel, with amino acids from site I and II highlighted with green and pink, while amino acids from RANKL-A and RANKL-B are presented as yellow and blue letters, respectively.

The RANKL–OPG binding interface presents two anchorage sites, named site I and II (Fig. 1). At site I, the 50s loop (CDR2) from OPG is placed along a groove in RANKL, forming patches of relatively small and separate contacts. Conversely, site II presents the 90s loop (CDR3) from OPG, deeply inserted into the groove surrounded by specific loops from neighbouring RANKL monomers, establishing a continuous patch of interactions.[10]

The available structural and biochemical data have suggested that site II is the major binding determinant of RANKL for the anchorage of OPG and RANK, despite subtle differences in a few interactions. Structural analysis of human and murine complexes of RANKL with OPG and RANK, respectively, has demonstrated that OPG exerts its decoy receptor function by directly occupying site II and blocking the access to key interacting residues, such as R223, Y241, and K257 in human RANKL.[10,47] The importance of key residues involved in the interaction between RANKL and OPG has been determined based on biochemical and biological assays, such as surface plasmon resonance, site-directed mutagenesis, and osteoclast differentiation assays.[10,47] Nevertheless, detailed energetic characterization of the PPI involved in the complex is not yet available, and would provide important information about the inhibition process and assist the design of new therapeutic molecules for the treatment of bone-related diseases.[49] In this context, the purpose of this work is to allow a deeper understanding of the RANKL–OPG interface within a quantum biochemistry framework.

Quantum biochemistry methods are important tools when a relatively qualitative estimate of binding affinities is required, being frequently used to describe systems with tens up to thousands of atoms within the scope of divide-to-conquer methodologies.[50–53] Despite the complexity of biological systems, increasing computational power, combined with recent developments in density functional theory (DFT),[54,55] has allowed the application of quantum biochemistry (frequently combined with classical molecular mechanics techniques) to study biological issues, such as enzymatic reactions and binding processes mediated by proteins.[56,57] For these systems, fragment-based methods were also developed to accelerate the calculations, seeking a balance between the computational cost and the accuracy required to produce trustworthy results.[58,59] These methods enable the computational treatment of large molecules or molecular systems, reaching consistent descriptions at the quantum biochemistry level. The principle is to divide the molecule of interest into fragments, employ a quantum biochemistry approach to calculate some properties of each fragment, and then combine the results to predict the same properties for the whole.[60] Within this picture, it was possible to describe the inactivation of ovine cyclooxygenase-1 by bromoaspirin and aspirin;[61] statin inhibition effectiveness in HMG-CoA reductase;[62] human dopamine D3 receptor interaction with the selective antagonist eticlopride and the inverse agonist haloperidol;[63,64] the activation and antagonism strength of an AMPA-sensitive glutamate receptor;[65] the investigation of willardine partial agonism in AMPA receptors;[66] the binding of isoniazid NADH adduct to InhA reductase,[67] and ibuprofen transportation by human serum albumin,[68] as well as estimating the residue–monomer and residue–residue interaction energies of the triple helix structure of collagen-like peptide T3-785.[69]

Moreover, an important feature to be considered during biological system simulations is a better description of the electrostatic effects. Almost all biological processes are controlled or modulated by electrostatic effects, which crucially demands the ability to perform accurate electrostatic calculations to describe quantitative structure–function correlation in proteins.[70] According to Schutz and Warshel (2001) electrostatic effects on biological systems play many roles, being present in enzyme catalysis, electron transfer, proton transport, ion channeling, ligand binding, macromolecular assembly, and signal transduction.[71] The electric charge pattern in a protein gives rise to electrostatic effects, which are described by an inhomogeneous dielectric function $\varepsilon(r)$, where r is the spatial coordinate describing the 3D structure of the protein. Generally, the dielectric function of the protein is assumed to be constant, within a mean field approximation, and various values have been chosen for it, usually in the range 4–40.[72] Small values for the dielectric constant ($\varepsilon < 10$) are associated with hydrophobic patches or cavities, like binding pockets, while large values of dielectric constants ($\varepsilon = 20$, $\varepsilon = 40$, or $\varepsilon = 80$) are associated with solvated hydrophilic patches and metal binding sites.[45]

Here, we take full advantage of the 2.7 Å resolution X-ray structure of the human RANKL–OPG complex (PDB ID: 3URF) to employ quantum methods, in order to investigate the individual energetic contribution of all interactions established in the complex.[10] The DFT formalism was chosen to estimate the binding energies within the molecular fractionation with conjugate caps (MFCC) framework,[38,50,51] a methodology specifically designed to facilitate the quantum biochemistry description of protein systems.[50] Moreover, explicit water molecules were considered in the calculations in two different ways, composing the molecular caps or as part of the analysed residues, in order to precisely estimate their effect on the binding energies. Furthermore, implicit water effects were considered by assuming two different values for the RANKL–OPG dielectric constant ($\varepsilon = 10$ and $\varepsilon = 40$) in the computations.

Our quantum calculations provide a detailed profile of all the PPIs involved in the RANKL–OPG interaction, presenting important information about the complex organization. The obtained results confirm the previously reported importance of residues such as R223 and K257 (but deny others, such as Y241), as well as reinforcing the importance of neglected residues, such as K181 and R224.[10] Additionally, the impact of a specific mutation in the development of Paget's disease is explained through a comparison between the non-mutant and mutant residue contribution to the RANKL–OPG binding energy.[47] Finally, previously proposed OPG-based peptides targeting the RANKL–OPG complex have also been analysed with respect to their binding energy to RANKL, corroborating the critical role of a few interactions. Therefore, the obtained results establish a quantum biochemistry-based picture of the inhibition mechanism exerted by OPG on RANKL within a binding energy framework, going beyond a strict distance-based analysis of the complex, as furnished by the crystallographic data, thus providing important new and quite relevant information for the design of new peptides for the treatment of osteopenic conditions.

2. Computational details

2.1. Structural data

The input data for the simulations was the 2.7 Å resolution structure of the human RANKL–OPG complex (PDB ID: 3URF), obtained by X-ray crystallography.[10] The asymmetric unit of the crystal structure is composed of one OPG molecule (truncated version) bound to a single RANKL monomer. Nevertheless, the RANKL trimer (biological assembly) can be generated by symmetry operations. OPG monomers are visualized in the complex bound to the grooves formed between RANKL monomers, establishing a 1 : 1 ratio between RANKL and OPG. Based on this complex, the model used for the calculations was composed of a single OPG monomer bound to two RANKL units, as observed in Fig. 1.

2.2. Classical and DFT calculations

Initially, hydrogen atoms were added to fill any dangling bonds in the X-ray structure and their positions were optimized using classical molecular mechanics, with non-hydrogen atoms being kept frozen. The optimization procedure was carried out with the software NAMD using the CHARMM force field, which has specific parameters for amino acids.[73] The convergence threshold parameters were chosen as: 2.0×10^{-5} kcal mol^{-1} for the total energy variation, 0.001 kcal mol^{-1} Å^{-1} for the maximum force per atom, and 1.0×10^{-5} Å for the maximum atomic displacement.

DFT simulations on the classically optimized structures were performed using DMOL3 code, implemented in Materials Studio, adopting the dispersion correction GGA + D (generalized gradient approximation) exchange–correlation functional, which is adequate to describe systems where hydrogen bonds and dispersive forces, such as van der Waals interactions, are present.[74] To model the dispersive forces, a state-of-the-art semi-empirical correction scheme proposed by Tkatchenko and Scheffler (TS) was adopted.[75] A double numerical plus polarization (DNP 4.4) basis set was chosen to expand the Kohn–Sham orbitals within an all-electron treatment scheme. The orbital cutoff for these computations was set to 3.7 Å, and a total energy variation smaller than 10^{-6} Ha was imposed as a threshold to achieve self-consistency.

2.3. The MFCC scheme

A detailed description of all PPIs stabilizing the interface of the complex RANKL–OPG was performed by quantum mechanics calculations. For this purpose, the MFCC scheme (molecular fractionation with conjugated caps) was applied, which is a very useful approach that provides an accurate description of biological systems through quantum calculations without a very high computational cost.[76] A method modified by Rodrigues and co-workers (2013) was applied to describe protein–protein interactions;[69] this calculates the interaction energy between two specific residues (R_i and R_j) according to

$$E_I(R_i\text{–}R_j) = E(C_{i-1}R_iC_{i+1}C_{j-1}R_jC_{j+1}) - E(C_{i-1}R_iC_{i+1}C_{j-1}C_{j+1}) - E(C_{i-1}C_{i+1}C_{j-1}R_jC_{j+1}) + E(C_{i-1}C_{i+1}C_{j-1}C_{j+1}) \quad (1)$$

In the above equation, the C_k terms refer to the conjugate caps, which must be chosen carefully to reproduce the local electronic environment of the amino acid residues.[53] In our study, these caps are the residues covalently bound to R_k; $C_{k\pm1} = R_{k\pm1}$ plus hydrogen atoms placed at any dangling bonds. At the right-hand side of eqn (1), the first term, $E(C_{i-1}R_iC_{i+1}C_{j-1}R_jC_{j+1})$, is the total energy of the system formed by two interacting capped residues. The second term, $E(C_{i-1}R_iC_{i+1}C_{j-1}C_{j+1})$, gives the total energy of the system formed by the capped residue R_i and the hydrogenated caps of R_j. The third term, $E(C_{i-1}C_{i+1}C_{j-1}R_jC_{j+1})$, is the total energy of the system formed by R_j and the set of caps of R_i. Finally, $E(C_{i-1}C_{i+1}C_{j-1}C_{j+1})$ is the total energy of the system formed by the caps only.[69]

Following this scheme, structural files (protein data bank format) were prepared and used as input for calculations with DMOL3 code (ESI Fig. S1†).[74] The total energies obtained for each system were then inserted in the above equation to determine the interaction energy between a specific pair of amino acid residues.

2.4. BIRD panel

The energy contribution of all the PPIs involved in the RANKL–OPG complex, as well as the individual contributions of specific amino acid residues, are plotted in BIRD panels – an acronym for Binding site, Interaction energy and Residues Domain. The BIRD panel depicts, concisely: (i) the interaction energy (in kcal mol^{-1}) between a specific pair of residues (or the energetic contribution of an specific amino acid residue), employing horizontal bars, from which one can assess the importance of each interaction/residue in the complex formation, whether attractive (negative energy) or repulsive (positive energy); (ii) the binding interface radius to which each interaction/residue belongs, at the right side; and (iii) the influence of the assigned value of the dielectric constant, depicted using distinct horizontal bars.[39–42,56]

2.5. RANKL–OPG interaction energy calculations

The energy contributions of all the PPIs involved in the RANKL–OPG complex were computed, considering a distance-based binding interface. For this purpose, all RANKL residues placed at a maximum distance of 4.0 Å from the OPG's surface were initially identified and then used as a reference for mapping an imaginary sphere of 4.0 Å. Afterwards, any residue belonging to the OPG with least one atom present inside the sphere was selected, thus determining all pairs of interacting residues in the complex. The selected top distance was based on an average estimate that takes into account the fact that binding interactions in protein systems tend to become negligible at distances higher than 4.0 Å.[77]

2.6. Waters and dielectric constant

Crystallographic water molecules disposed within a range of 4.0 Å from the analysed residues were considered in the calculations, with the aim of deeply exploring their influence over the binding energy estimates. Each water molecule was embedded uniquely in the closest residue in the pair of interactions, and its influence was explored through two different treatments. The first treatment has considered water molecules as additional caps (treatment 1), beyond the covalently bound residues, while the second treatment has considered these molecules as part of the analysed residues (treatment 2). This strategy is meant to describe with accuracy the chemical environment of each analysed amino acid residue, providing a comparative basis for the contribution of water molecules over binding energies on the protein interface.

All interaction energy calculations were performed using the COSMO continuum solvation model, *i.e.* an implicit water representation, $\varepsilon = 10$ and $\varepsilon = 40$.[78,79] These values are in agreement with the results of the work of Vicatos *et al.*, who have investigated the absolute folding free energies in a diverse set of 45 proteins, finding that the best fitted values of the dielectric constant for charge–charge interactions and for self-energies are in the range $1 < \varepsilon < 40$.[79] Currently, the application of the COSMO continuum solvation model is a physically reasonable and also practical solution.[80] Warshel and co-workers (1984) have shown that any model with a large dielectric constant for charge–charge interactions will usually looks like an excellent model in cases with surface groups.[81] In addition, Antony and Grimme (2012) considered the inclusion of the crystallographic water molecules into the fractionation scheme as the next step to improve the efficiency of GGA-based DFT energy calculations of full protein-ligand interactions.[80] Recently, it was shown that a value assigned to the dielectric constants of human serum albumin and the laccase enzyme can influence the binding pattern of the anti-inflammatory, ibuprofen, in the former case,[68] and the pesticide, formetanate, in the latter.[82]

2.7. *In silico* mutagenesis

The energetic impact of the single mutation responsible for Paget's disease, which replaces a phenylalanine residue by a leucine at position 96 (F96L) in OPG, was investigated through *in silico* mutagenesis and quantum calculations. *In silico* mutagenesis was carried out with the VMD (Visual Molecular Dynamics) software, using the human RANKL–OPG complex as template. After replacing residue F96 for leucine in the OPG structure, hydrogens were added to the whole complex to fill any dangling bonds and optimized along with the heavy atoms of the mutant residue with NAMD, using the CHARMM force field.[73,83]

2.8. Molecular docking of the peptides

The binding analysis of the complexes between RANKL and two previously reported inhibitory peptides, designed based on OPG's sequence, was explored by molecular docking calculations. The selected peptides, named OP3-4 and YR-11, both presenting 11 amino acids, were able to inhibit RANK activity at around 90 and 93%, respectively. While YR-11 (YCEIEFCYLIR) presents a linear structure, (YLEIEFSLKHR), OP3-4, is a cyclic peptide (linked by a disulfide bridge); these both differ from OPG's natural sequence by one and four residues (highlighted in bold), respectively.[84,85]

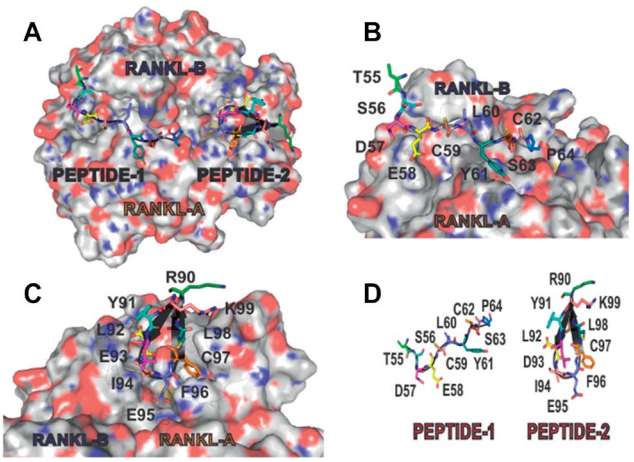

Fig. 2 Peptides 1 and 2. (A) General representation of peptides 1 and 2 over RANKL surface. (B) and (C) Amino acid composition of peptides 1 and 2 and their disposal over binding sites I and II. The peptides are represented as colored sticks over a transparent black cartoon, while RANKL is represented as a surface (positive, negative and neutral spots are colored in blue, red and grey, respectively). (D) Individual representation of peptides 1 and 2.

Molecular docking calculations were performed with AutoDock Vina, version 1.1.2, which applies an iterated local search global optimizer for the optimization procedure. The succession of each step consists of a mutation and local optimization, with the acceptance decisions made according to the Metropolis criterion. This uses the efficient quasi-Newton method, Broyden–Fletcher–Goldfarb–Shanno (BFGS) for local optimization.[86] The Autodock graphical interface, AutoDockTools, version 1.5.6, was used to retain polar hydrogens and add partial charges to the proteins and ligands using the Kollman united charges.[61] The receptor (RANKL) and ligands (peptides) were treated as rigid and flexible molecules, respectively. The search space for the docking calculations was defined by a 20 Å × 20 Å × 20 Å cube centred on binding site II. Exhaustiveness was set to 15, and all other parameters were used as default. For each ligand, the ten top-ranked generations based on the predicted binding affinity (in kilocalories per mole) were analysed. The solutions were first chosen based on the coordination of the crystal structure for peptide-2, and then the most suitable results were further ranked based on the theoretical binding energy (given as a negative score in kcal mol^{-1}).

Table 1 Individual energetic contributions of RANKL's amino acid residues involved in OPG recognition

Unit	Residue	Site	T1:ε=10	T1:ε=40	T2:ε=10	T2:ε=40
RANKL A	Y188	I	-1	-1	-1	-1
RANKL A	R191	I	-14	-9	-14	-10
RANKL A	G192	I	-5	-4	-5	-4
RANKL A	R223	II	-15	-7	-15	-7
RANKL A	H224	II	-1	-1	-1	-1
RANKL A	H225	II	-8	-9	-22	-17
RANKL A	F270	II	-6	-6	-6	-6
RANKL A	H271	II	-1	-1	-1	-1
RANKL A	F272	II	-3	-3	-2	-3
RANKL A	Q303	I	-2	-2	-2	-2
RANKL B	S179	II	12	12	11.2	11.9
RANKL B	H180	II	4	5	0	1
RANKL B	K181	II	-20	-11	-16	-11
RANKL B	Q237	II	19	21	17.1	20.7
RANKL B	M239	II	-9	-8	-9	-8
RANKL B	Y241	II	7.4	7.1	7.4	7.1
RANKL B	I249	I	-2	-1	-2	-1
RANKL B	H253	I	-1	0	-1	0
RANKL B	K257	II	-11	-7	-11	-6
RANKL B	T261	II	-1	0	-1	0
RANKL B	K282	I	-13	-5	-12	-5
RANKL B	R284	I	-23.2	-7.6	-23.2	-7.6
RANKL B	S294	II	-2	-2	-2	-2
RANKL B	N295	II	0	0	-2	-2

3. Results and discussion

3.1. Overall characterization

The quantum biochemistry study of the human RANKL–OPG complex was initialized using the X-ray crystal structure deposited in PDB by Nelson *et al.* (2012).[47] For the purpose of clarity, the RANKL units have been identified as monomers A (RANKL-A) and B (RANKL-B), (see Fig. 2).

DFT calculations were employed to assess the relative energetic contribution of each pair of interactions, as well as the individual contribution of each amino acid residue, at binding sites I and II, from the RANKL–OPG complex.[87] As described above, treatments one and two were applied aiming to further analyse the influence of water molecules over energy estimates. Nevertheless, the current discussion will focus solely on treatment 1 (T1:$\varepsilon = 10$ and T1:$\varepsilon = 40$ for dielectric constants of 10 and 40, respectively), presenting treatment 2 (T2:$\varepsilon = 10$ and T2:$\varepsilon = 40$ for dielectric constants of 10 and 40, respectively) as supplementary material.

The current strategy, using a distance-based binding interface (top distance of 4.0 Å), has found a few extra residues on RANKL, beyond those previously mentioned in the literature, composing binding sites I and II.[10,47] Therefore, for RANKL, site I is composed of residues Y188, D190, R191, G192, K248, I249, H253, K282, R284, P301, D302, and Q303, while site II presents residues S179, H180, K181, R223, H224, H225, T227, Q237, M239, Y241, K257, T261, F270, H271, F272, S294, and N295 (newly identified residues highlighted in bold) (Table 1). In the case of OPG, the current approach has confirmed all previously described residues for sites I (H47, Y48, S56, E58, L60, Y61, P64, and V65) and II (K67, E68, L69, R90, Y91, L92, E93, I94, E95, F96, C97, L98, and K99) (Table 2). As described earlier, OPG interacts with RANKL at binding sites I and II mainly through loops 50s and 90s, respectively, which represent linear fragments of the protein structure.[10,47] Based on this, we have named here as peptides 1 and 2 the protein fragments from OPG corresponding to loops 50s (T55–P64) and 90s (R90–K99), respectively, which directly interact with RANKL (Fig. 2).

3.2. Binding site analysis

Through a structural analysis of binding site I, twenty-two pair of interactions were detected within a range of 4.0 Å, which were almost exclusively attractive (Fig. 3, Table 3, ESI Fig. S2 and S3†). Despite not being very expressive (with a maximum value of -14.0 kcal mol^{-1} for K248–S56 with T1:$\varepsilon = 10$) they create a suitable environment for the anchorage of peptide-1, which is placed almost parallel to the groove formed between RANKL units.[10] Thus, the sum of all interactions at site I (most attractive below -10 kcal mol^{-1}) generates a considerably high binding energy (-70.5 and -33.9 kcal mol^{-1}, for T1:$\varepsilon = 10$ and T1:$\varepsilon = 40$, respectively), which favours the complex stability (Fig. 9). The three most energetically significant residues of peptide-1 for OPG binding are Y48, D57, and E58, with individual contributions of -10.0, -9.2, and -27.0 kcal mol^{-1} (T1:$\varepsilon = 10$), respectively (Fig. 4 and 5). Nevertheless, these residues do not present a remarkable influence over the complex formation (not individually), as confirmed by site-directed mutagenesis, SPR and osteoclast differentiation assays.[10] Despite the considerable energy contribution of residues, such as E58, none of them

Table 2 Individual energetic contributions of OPG's amino acid residues involved in RANKL recognition

Residue	Site	T1:$\varepsilon = 10$	T1:$\varepsilon = 40$	T2:$\varepsilon = 10$	T2:$\varepsilon = 40$
H47	I	−4	−1	−5	−2
Y48	I	−10	−9	−9	−9
Y49	I	1	1	1	1
S56	I	6	5	6	5
D57	I	−9.2	−2.6	−9.2	−2.6
E58	I	−27	−10	−26	−10
L60	I	−4	−2	−4	−2
Y61	I	−8	−5	−7	−5
S63	I	−1	−1	−1	−1
P64	I	−3.3	−2.7	−3.8	−3.3
V65	I	−3	−3	−3	−4
K67	I/II	14	7	11	8
E68	II	−7	−2	−8	−2
L69	II	−1	−4	−2	−4
R90	II	−2.5	−0.7	−3.5	−0.7
Y91	II	0	0	−1	0
L92	II	−1	0	1	−1
E93	II	19	19	17.4	17.5
I94	II	−3	−1	−7	−5
E95	II	−38.6	−8.9	−36.7	−7.8
F96	II	−15	−15	−21	−21
C97	II	−2	−3	−7	−5
L98	II	−5	−2	−5	−2
K99	II	−2	0	−2	0

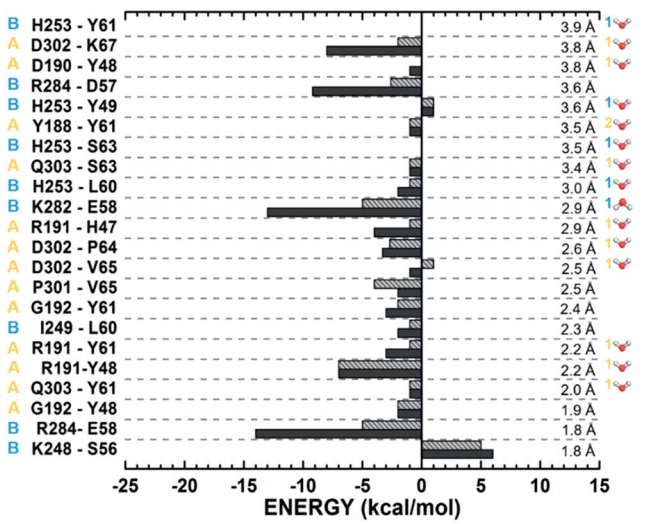

Fig. 3 Binding site, interaction energy, and residues domain (BIRD) panel showing the MFCC interaction energy for all interactions established between RANKL and OPG at site I, applying treatment 1. Dark and light grey bars represent values obtained with $\varepsilon = 10$ and $\varepsilon = 40$, respectively. Colored letters at the left side of the panel assign the RANKL unit involved for each interaction. The distance and the number of water molecules involved for each interaction are presented at the right side of the panel. Numbers disposed at the left side of the water representation are related to RANKL residues, while numbers disposed at the right side are related to OPG residues.

Table 3 Individual energetic contributions of all interactions involved in site I[a,b]

RANKL – OPG	Distance (Å)	T1:ε=10	T1:ε=40	T2:ε=10	T2:ε=40
B K248 - S66	1.8	6	5	6	5
B R284 - E58	1.8	-14	-5	-14	-5
A G192 - Y48	1.9	-2	-2	-2	-2
A Q303 - Y61	2	-1	-1	-1	-1
A R191 - Y48	2.2	-7	-7	-7	-7
A R191 - Y61	2.2	-3	-1	-2	-1
B I249 - L60	2.3	-2	-1	-2	-1
A G192 - Y61	2.4	-3	-2	-3	-2
A P301 - V65	2.5	-2	-4	-2	-4
A D302 - V65	2.5	-1	1	-1	0
A D302 - P64	2.6	-3.3	-2.7	-3.8	-3.3
A R191 - H47	2.9	-4	-1	-5	-2
B K282 - E58	2.9	-13	-5	-12	-5
B H253 - L60	3	-2	-1	-2	-1
A Q303 - S63	3.4	-1	-1	-1	-1
B H253 - S63	3.5	0	0	0	0
A Y188 - Y61	3.5	-1	-1	-1	-1
B H253 - Y49	3.6	1	1	1	1
B R284 - D57	3.6	-9.2	-2.6	-9.2	-2.6
A D190 - Y48	3.8	-1	0	0	0
A D302 - K67	3.8	-8	-2	-10	-1
B H253 - Y61	3.9	0	0	0	0

[a] **A** – RANKL-A residues. [b] **B** – RANKL-B residues.

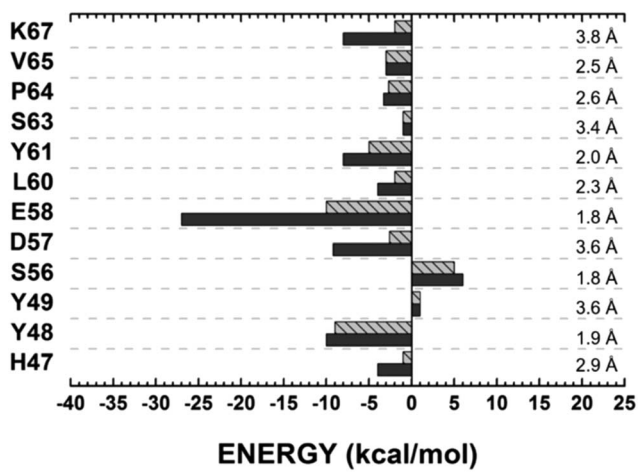

Fig. 4 Binding site, interaction energy and residues domain (BIRD) panel showing the MFCC interaction energy for all OPG's amino acid residues involved in site I, applying treatment 1. Dark and light grey bars represent values obtained with $\varepsilon = 10$ and $\varepsilon = 40$, respectively. The distance of each interaction is presented at the right side of the panel.

seems to directly interfere with RANK association, which interacts with RANKL mainly through a patch equivalent to binding site II.[11] These facts emphasize a secondary role for site I over OPG binding and functionality, mostly supporting proper insertion of the 90s loop (binding site II), which presents residues that in fact block the main binding site of RANK on the RANKL surface. Furthermore, this role is reinforced by the existence in site I of a collaborative association among several other minor attractive interactions, which individually possess little influence over OPG binding. Based on this, we can assume that amino acid residues with crucial influence over OPG binding must present not only considerable binding energies, but also the ability to block important interactions associated with the establishment of the RANK–RANKL complex.

In the case of binding site II, forty-two interactions are present within a range of 4.0 Å, disposed in a much more intricate net. Unlike site I, the presence of a comparable number of attractive and repulsive interactions confers to site II a considerably lower total binding energy (−38.1 and −24.0 kcal mol^{-1}, applying T1:$\varepsilon = 10$ and T1:$\varepsilon = 40$, respectively) (Fig. 6 and 10, and ESI Fig. S4 and S5†). However, the number and

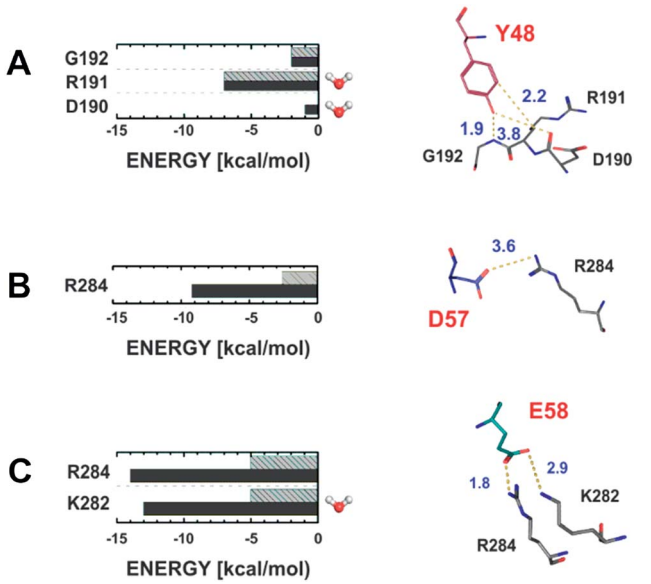

Fig. 5 Main amino acid residues involved in peptide 1 anchorage. The binding site, interaction energy and residues domain (BIRD) panels placed at the left side present the MFCC interaction energy for each interaction performed by Y48 (A), D57 (B), and E58 (C). Dark and light grey bars represent values obtained with $\varepsilon = 10$ and $\varepsilon = 40$, respectively. The residue coordinations are represented at the right side as sticks, with the main interactions represented as yellow dashed lines (distances are indicated in Å). Water representations at the right side of the BIRD panels indicate interactions involving water molecules.

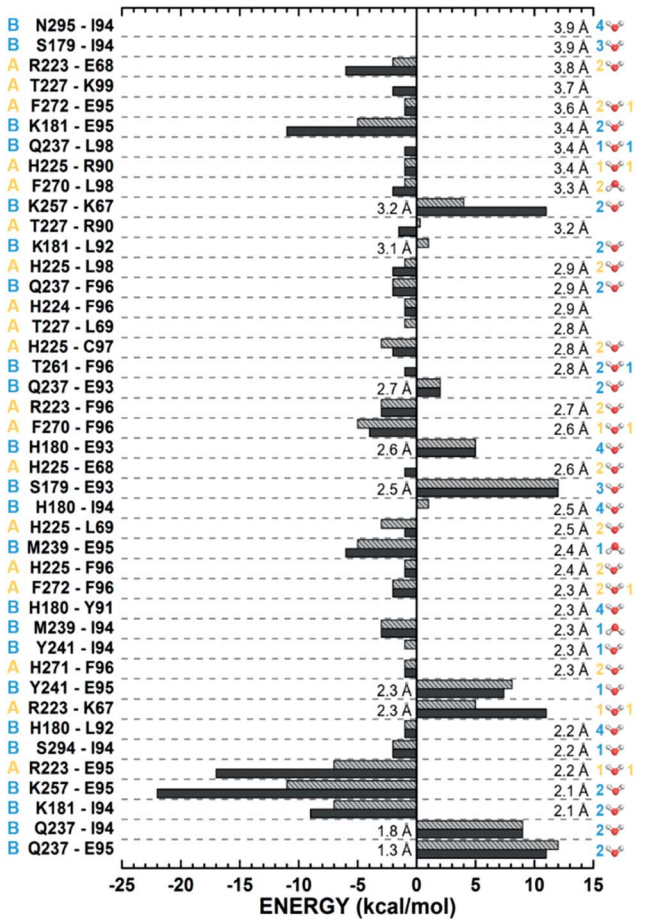

Fig. 6 Binding site, interaction energy and residues domain (BIRD) panel showing the MFCC interaction energy for all interactions established between RANKL and OPG at site II, applying treatment 1. Dark and light grey bars represent values obtained with $\varepsilon = 10$ and $\varepsilon = 40$, respectively. Colored letters at the left side of the panel assign the RANKL unit involved for each interaction. The distances related to attractive and repulsive interactions are presented at the right side and at the central part of the panel, respectively. The water molecules involved in each interaction are represented at the right side of the panel, with numbers disposed at the left of the water representation side related to RANKL residues and numbers disposed at the right side related to OPG residues, respectively.

importance of all interactions, determined by quantum calculations, corroborate their critical role for the RANKL–OPG complex (Table 4).[10] In peptide-2, the most energetically important residues are I94, E95, and F96, with individual contributions of −3.0, −38.6, and −15.0 kcal mol^{-1} (T1:$\varepsilon = 10$), respectively, comprising more than a half of all interactions established in site II (Fig. 6, 7, and 8, and ESI Fig. S6†). These results agree with previous biological assays and attest the importance of this tripeptide in OPG binding and its inhibitory activity (Fig. 7 and 8).

Complementarily, quantum calculations have indicated R191, K282, and R284 as the energetically most relevant residues at site I, and K181, R223, and K257 at site II, for OPG recognition by RANKL (ESI Fig. S6–S9†). These residues are potential templates for alternative approaches focused on designing peptides targeting RANK instead of RANKL, aiming to block key residues on RANK's surface for the complex formation. Recently, peptides based on the RANKL structure (RANK antagonist) were proposed to specifically block RANK–RANKL interactions.[88] Nevertheless, these RANKL-based peptides presented a lower efficiency over osteoclast differentiation when compared to OPG or OPG-based peptides.[84,85,88] Interestingly, these antagonist peptides were designed not to target the binding sites between RANK and RANKL, but a hinge region between two cysteine-rich domains on RANK, which is responsible for the conformational change upon RANK association.[89] Therefore, efficient inhibition of osteoclastogenesis seems to hinge on the proper blockage of key PPIs in the RANK–RANKL complex.

Interestingly, the energy analysis revealed that calculations involving a dielectric constant of 10 ($\varepsilon = 10$) generate increased (sometimes significantly) binding values (attractive or repulsive) for polar interactions when compared to a dielectric constant of 40 ($\varepsilon = 40$). However, the same is not true for hydrophobic interactions, which eventually present slightly increased values for treatments, considering $\varepsilon = 40$. The values of dielectric constants used in this work ($\varepsilon = 10$ and $\varepsilon = 40$) are representative enough to consider the inhomogeneous nature of protein interfaces, which may include a great number of polar, charged, and hydrophobic residues. Protein systems may include patches presenting variable values of the dielectric

Table 4 Individual energetic contributions of all interactions involved in site II[a,b]

RANKL – OPG	Distance (Å)	T1:ε=10	T1:ε=40	T2:ε=10	T2:ε=40
B Q237 - E95	1.3	11	12	10.9	12.1
B Q237 - I94	1.8	9	9	9	9
B K181 - I94	2.1	-9	-7	-7	-6
B K257 - E95	2.1	-22	-11	-21	-10
A R223 - E95	2.2	-17	-7	-17	-7
B S294 - I94	2.2	-2	-2	-2	-2
B H180 - L92	2.2	-1	-1	0	-1
A R223 - K67	2.3	11	5	11	5
B Y241 - E95	2.3	7.4	8.1	7.4	8.1
A H271 - F96	2.3	-1	-1	-1	-1
B Y241 - I94	2.3	0	-1	0	-1
B M239 - I94	2.3	-3	-3	-3	-3
B H180 - Y91	2.3	0	0	-1	0
A F272 - F96	2.3	-2	-2	-1	-2
A H225 - F96	2.4	-1	-1	-7	-7
B M239 - E95	2.4	-6	-5	-6	-5
A H225 - L69	2.5	-1	-3	-2	-3
B H180 - I94	2.5	0	1	-3	-2
B S179 - E93	2.5	12	12	12.2	11.9
A H225 - E68	2.6	-1	0	-2	0
B H180 - E93	2.6	5	5	4	4
A F270 - F96	2.6	-4	-5	-4	-5
A R223 - F96	2.7	-3	-3	-3	-3
B Q237 - E93	2.7	2	2	1.2	1.6
B T261 - F96	2.8	-1	0	-1	0
A H225 - C97	2.8	-2	-3	-7	-5
A T227 - L69	2.8	0	-1	0	-1
A H224 - F96	2.9	-1	-1	-1	-1
B Q237 - F96	2.9	-2	-2	-3	-2
A H225 - L98	2.9	-2	-1	-2	-1
B K181 - L92	3.1	0	1	1	0
A T227 - R90	3.2	-1.5	0.3	-1.5	0.3
B K257 - K67	3.2	11	4	10	4
A F270 - L98	3.3	-2	-1	-2	-1
A H225 - R90	3.4	-1	-1	-2	-1
B Q237 - L98	3.4	-1	0	-1	0
B K181 - E95	3.4	-11	-5	-10	-5
A F272 - E95	3.6	-1	-1	-1	-1
A T227 - K99	3.7	-2	0	-2	0
A R223 - E68	3.8	-6	-2	-6	-2
B S179 - I94	3.9	0	0	-1	0
B N295 - I94	3.9	0	0	-2	-2

[a] **A** – RANKL-A residues. [b] **B** – RANKL-B residues.

constant within the 4–80 interval, with a value of 80 representing a completely solvated environment.[45]

Additionally, treatment two (waters considered as part of the analysed residues) presents increased values for attractive interactions, especially those of lower significance. Thereby, we can conclude that this energy increment is a contribution of water molecules involved in these interactions, since treatment one considers it as part of the caps, which highlights its importance over the protein binding.

3.3. The tripeptide I94–E95–F96 as the key for OPG functionality

Quantum calculations have here attested the importance of binding site II over the RANKL–OPG complex formation, which has been experimentally explored before through different approaches.[10,47] Nevertheless, we report for the first time the critical role of the tripeptide segment, I94–E95–F96, from the OPG structure over its functionality based on the energy

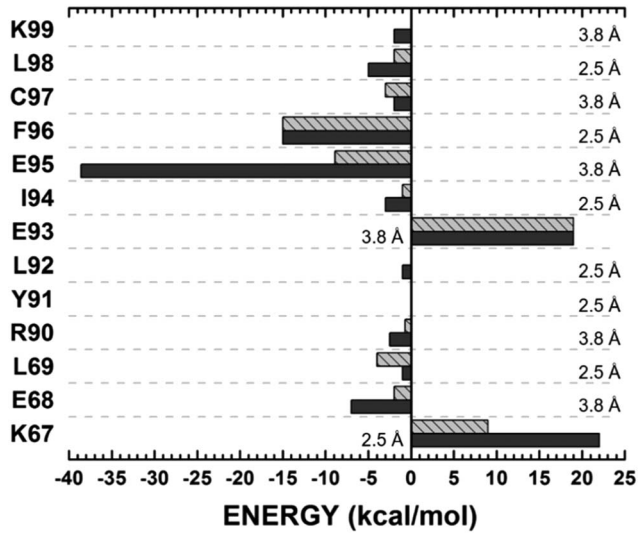

Fig. 7 Binding site, interaction energy and residues domain (BIRD) panel showing the MFCC interaction energy for all OPG's amino acid residues involved in site II, applying treatment 1. Dark and light grey bars represent values obtained with $\varepsilon = 10$ and $\varepsilon = 40$, respectively. The distances related to attractive and repulsive interactions are presented at the right side and at the central part of the panel, respectively.

analysis of all PPIs in the RANKL–OPG complex. This tripeptide is involved in 35.9% of all PPIs (23 of 46) detected within a range of 4.0 Å, contributing 53% of the total binding energy and 46.7% of the total attractive energy (Fig. 6 and Table 4). The importance of residues E95 and F96 was previously considered and analysed, although no reports have been made about using this tripeptide core as a template for designing inhibitory peptides.[10,47] Nevertheless, previous reports have considered the design of small molecules targeting RANKL residues, such as R223, Y241, and K257 (considered "hot-spots"), which interact with the tripeptide core, as a potential way to target the RANK–RANKL–OPG molecular triad.[10]

The key role of E95 was analysed by Luan and co-workers (2012), who proved the inability of an OPG mutant at this position (E95A) to act as an inhibitor of the osteoclast differentiation induced by RANK.[10] Now, our quantum calculations have indicated E95 as the energetically most important residue in the complex, which corroborates the available biological data. This residue is placed on the tip of the 90s loop, being inserted upon OPG binding into the bottom of the cavity built by RANKL units on site II. The most significant attractive interactions involving E95 are established with residues K181

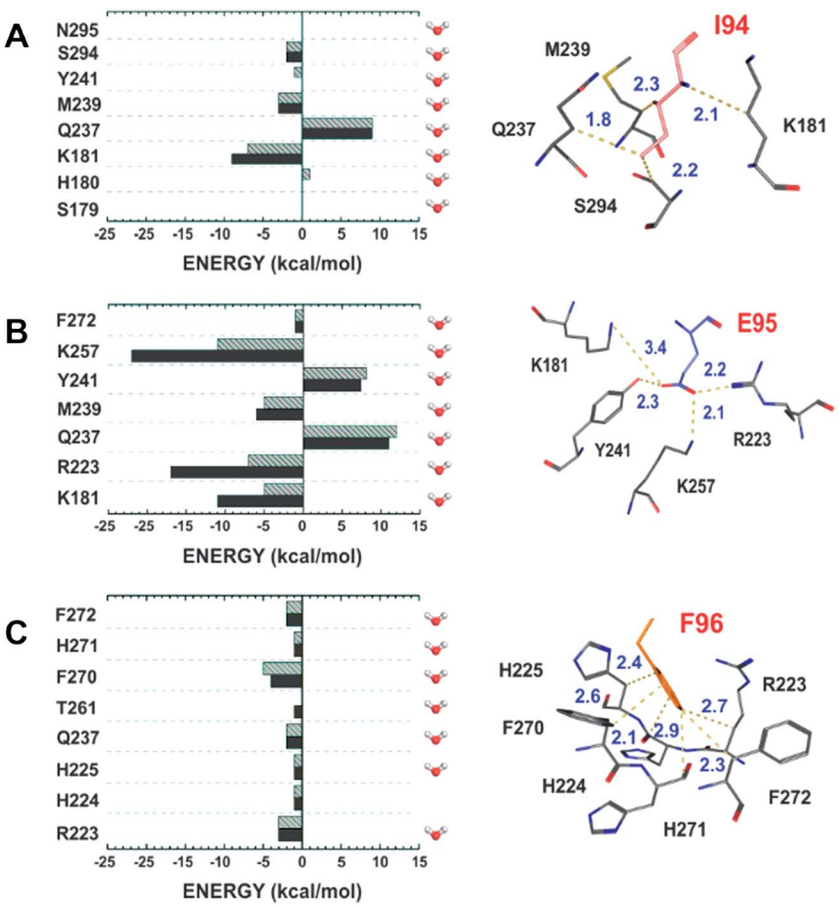

Fig. 8 Main amino acid residues involved in peptide 2 anchorage. The binding site, interaction energy and residues domain (BIRD) panels placed at the left side present the MFCC interaction energy for each interaction performed by I94 (A), E95 (B), and F96 (C). Dark and light grey bars represent values obtained with $\varepsilon = 10$ and $\varepsilon = 40$, respectively. The residue coordinations are represented at the right side as sticks, with the main interactions represented as yellow dashed lines (distances are indicated in Å). Water representations at the right side of the BIRD panels indicate interactions involving water molecules.

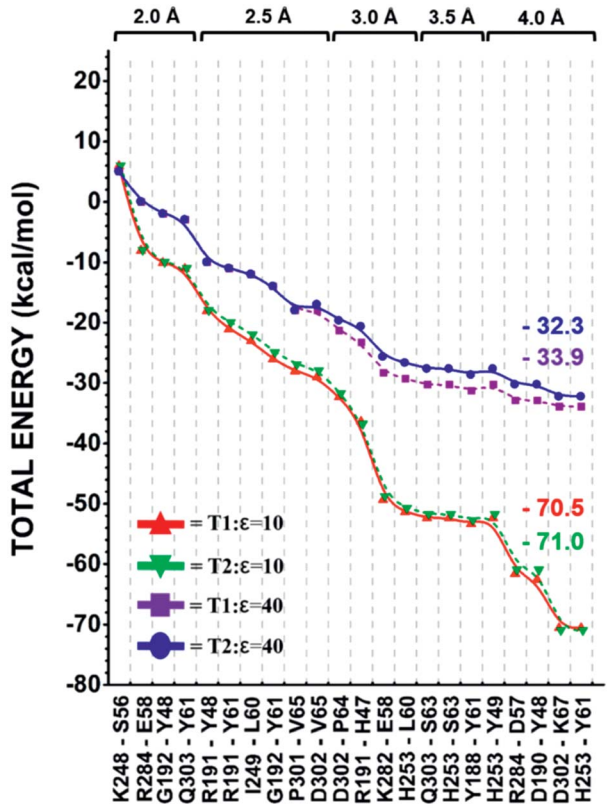

Fig. 9 Total interaction energy for site I as a function of distance, applying treatments 1 and 2 and distinct values of the dielectric constant. Energy values are represented as kcal mol^{-1}.

(RANKL-B), R223 (RANKL-A), and K257 (RANKL-B), and include the most important interactions in the complex. These interactions are directly dependent on two other repulsive ones established with residues Q237 and Y241 (both from RANKL-B), which induce proper coordination of the E95 side chain, as detailed later.

In the case of I94, despite presenting a low energetic contribution, this residue is essential for the coordination of peptide-2, allowing and assisting the blockage of key residues for RANK anchorage (Fig. 7 and 8). Attractive interactions are established through hydrophobic contacts with surrounding side chains, especially K181 (RANKL-B), while repulsive interactions arise from pairing to charged groups, such as those present on the Q237 side chain.

For F96, a structural comparison between the human RANKL–OPG and the hybrid mRANK–hRANKL complexes suggests that the pi-stacking interaction involving the phenyl group of this residue is critical for RANKL–OPG complex stabilization. Quantum calculations showed that F96 is the second energetically most important residue on peptide-2 (after E95), establishing attractive interactions to eight different RANKL residues, and forming a compact hydrophobic core (Fig. 7 and 8). Comparatively, these interactions are absent in the RANK–RANKL complex, this residue being replaced by a cysteine (C127) in the RANK structure.[47] Indeed, a sulphate ion occupies the position of the F96 side chain in the hybrid mRANK–hRANKL complex, indicating a lack of stabilizing interactions. This remarkable difference between RANK and OPG presents a strict correlation to the stronger binding performed by the latter with RANKL. This statement is reinforced by pathological conditions associated with mutations on this very residue, such as Paget's disease, in which a leucine residue replaces the original phenylalanine on the OPG structure (F96L), causing a disorder of accelerated bone resorption.[90]

3.4. Repulsive interactions and collaborative associations

The energy analysis of all the PPIs on the RANKL–OPG complex allows the observation at site II of the existence of a contributive association between attractive and repulsive interactions that favour complex stabilization (Table 4). As an example, we can mention residue K67 from OPG, which establishes considerable repulsive interactions with residues R223 and K257 from RANKL (each of 11 kcal mol^{-1}, with T1:$\varepsilon = 10$), which in turn generate the most attractive interactions at binding site II, both to residue E95 from OPG (-22 and -17 kcal mol^{-1}, respectively). Similarly, residue Q237 from RANKL also establishes a significant repulsive interaction to E95 (11 kcal mol^{-1}), inducing in the former a side chain conformation that optimizes the above-mentioned attractive interactions. Different residues at site II are involved in these repulsive/attractive associations, creating a "fingerprint" binding between OPG and RANKL, which diverges from the RANK–RANKL complex. Based on this, we can assume that repulsive interactions are not merely disturbing processes but present an important coordination function over specific residues, locking conformations that maximize attractive interactions.

3.5. Paget's disease – an energy perspective

Paget's disease is a rare autosomal recessive osteopathy characterized by debilitating fractures and deformities due to a markedly accelerated rate of bone remodelling throughout the skeleton.[90] Currently, it is well known that a single mutation affecting the OPG gene is responsible for Paget's disease in humans, which replaces a phenylalanine residue at position 96 by a leucine (F96L).[91] As mentioned before, F96 is a crucial residue for OPG binding and functionality, establishing important hydrophobic interactions to eight different RANKL residues (Fig. 7 and 8). The consequences derived from its substitution by a leucine residue are consistent with OPG dysfunction, indicating the disruption of these hydrophobic contacts as damaging for the complex stabilization, possibly accelerating its dissociation.[47]

Aiming to understand the structural basis of this severe condition, we performed *in silico* mutagenesis of the phenylalanine residue at position 96 by a leucine, followed by quantum calculations of the mutated residue to analyse the energy impact of this substitution. The structural analysis revealed that a leucine residue at this position on the OPG structure is able to establish only five interactions to RANKL residues, compared to eight performed by phenylalanine, despite presenting similar coordination of its side chain. Furthermore, most of these interactions are energetically less significant when compared to

those from phenylalanine, which generates for the latter a total binding energy that is twofold higher (Fig. 11a). Based on this, we can assume that substitutions at this position that may disrupt these hydrophobic contacts would significantly decrease the binding affinity of OPG for RANKL, which is in accordance with the available biological data, which reports an affinity 2900 times lower of the mutant OPG-F96L for RANKL, when compared to the wild-type protein.[47] In this way, quantum calculations have consistently described the energy impacts of this substitution over the complex, emphasizing the critical role of the tripeptide core, I94–E95–F96, for OPG biological function.

3.6. Structural simulations and energy analysis of inhibitory peptides

The importance of binding site II for RANKL–OPG complex formation and stabilization was previously described in the literature through structural and biological assays, being supported here by quantum calculations, which stressed the importance of the tripeptide core, I94–E95–F96, for OPG binding.[10,47] Accordingly, peptide-2 became a suitable template for designing inhibitory peptides specifically targeting the RANK–RANKL complex. Following this lead, several OPG-based peptides were proposed in the last decade as potential drugs for the treatment of osteopenias. Nevertheless, the design of these peptides was based solely on structural aspects of the RANKL–OPG complex, and most of them did not present significant efficiency in comparison to OPG.

However, two peptides among the several proposed have attracted attention due to their high inhibitory potential. These peptides were named YR-11 (YLEIEF**S**LKHR) and OP3-4 (Y**C**EIEF-**CYLI**R), both presenting 11 amino acid residues but with different structures, strictly based on loop 90s (Y91 to R101). YR-11 is a linear peptide presenting a single modification when compared to peptide-2, where a cysteine residue at position 7 (involved in a disulphide bridge with C86 on OPG) was replaced by a serine (highlighted in bold). On the other hand, OP3-4 is an exocyclic peptide (through a disulphide bridge between C2 and C7) presenting four sequence alterations in comparison to peptide-2 (highlighted in bold). In this sequence, a tyrosine residue replaces a leucine at position 8 and the original C-terminal residues, K9–H10, were replaced by L9–I10. The inhibitory effect of these peptides relies on the blockage of key residues on RANKL for RANK anchorage at binding site II, such as K181 and Y241, preventing receptor trimerization and consequently osteoclastogenesis.[84,85]

Molecular docking calculations were performed to simulate the complexes between RANKL and the proposed peptides, YR-11 and OP3-4. The best results obtained for both peptides presented the tripeptide core, I4–E5–F6 (corresponding to I94–E95–F96 on OPG), with coordinations almost identical to the crystal structure, which was used as a selection parameter. Based on the generated complexes, we could infer the influence of the alterations inserted on the peptide sequences over the binding to RANKL. In the case of YR-11, the presence of a serine residue on position 7 (instead of a cysteine) probably increases the peptide solubility and maximizes the polar contacts with H225 on RANKL. For OP3-4, Y8 maximizes the contacts with F270 and Q237 on RANKL, also enhancing the peptide stability through pi-stacking interactions with F6. Interestingly, the replacement in OP3-4 of the original C-terminal residues has increased the inhibitory potency of this peptide, which was attributed to a stronger interaction with RANKL.[85]

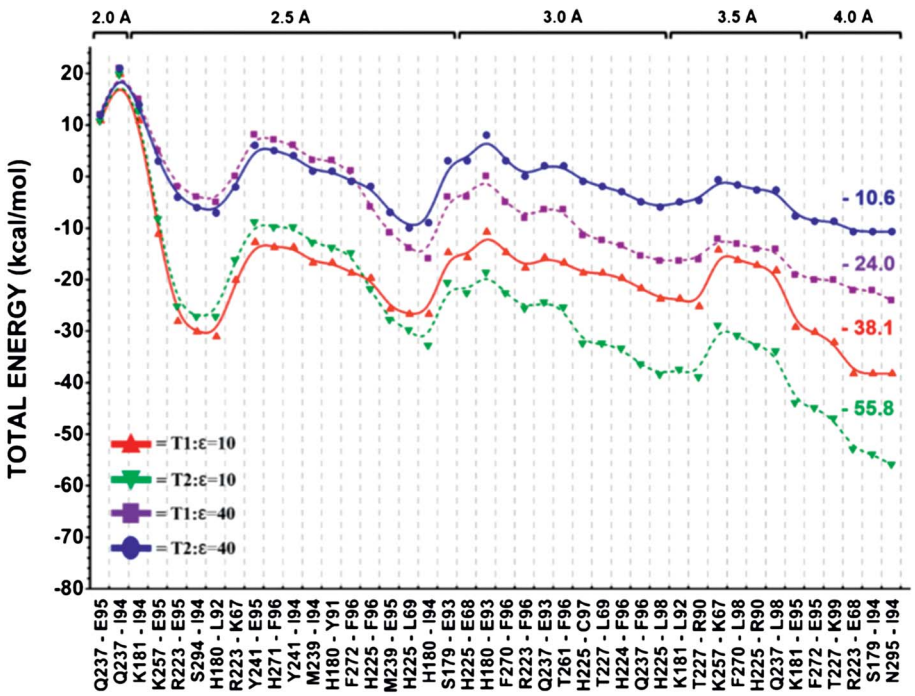

Fig. 10 Total interaction energy for site II as a function of distance, applying treatments 1 and 2 and distinct values of the dielectric constant. Energy values are represented as kcal mol^{-1}.

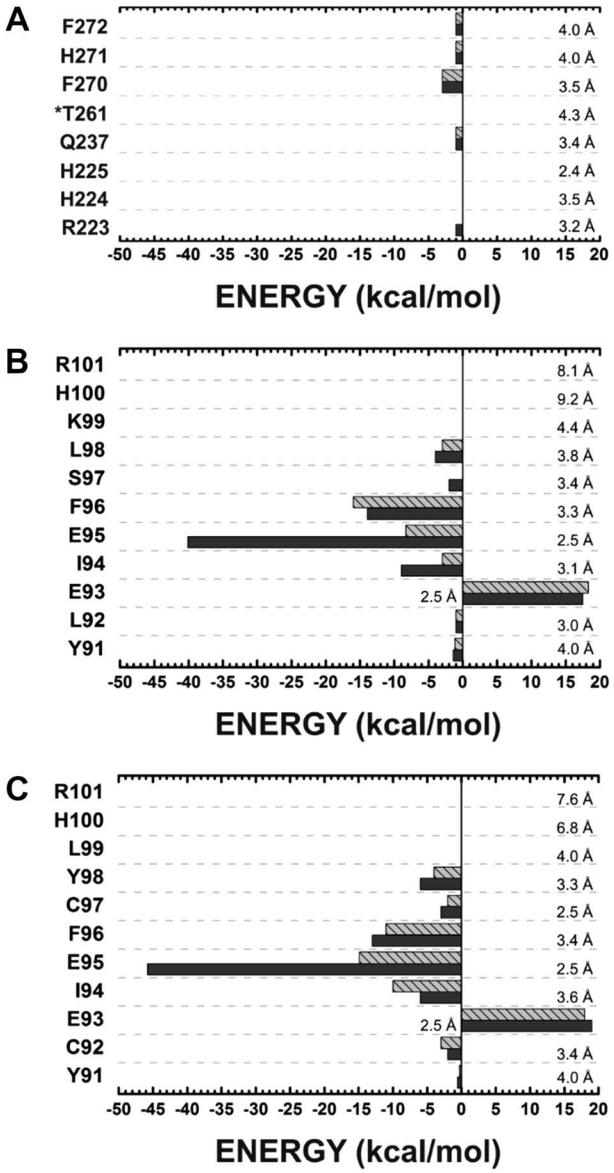

Fig. 11 Binding site, interaction energy and residues domain (BIRD) panel showing the MFCC interaction energy for all interactions established by the peptides YR-11 and OP3-4, and the mutated residues on OPG-F96L. (A) Energy analysis of the mutant residue L96 at site II, applying treatment 1. Interactions present for F96 on OPG but absent for the mutant residue on OPG-F96L are marked with *. (B) Energy analysis of peptide YR-11 at site II. (C) Energy analysis of peptide OP3-4 at site II. Dark and light grey bars represent values obtained with $\varepsilon = 10$ and $\varepsilon = 40$, respectively. The distances related to attractive and repulsive interactions are presented at the right side and at the central part of the panel, respectively.

After docking, a distance-based binding interface (within a range of 4.0 Å) was determined for both complexes to detect all interactions involved in the peptide binding to RANKL. Quantum calculations were also performed to analyse the energetic contribution of each peptide residue to the complex formation. Following this strategy, no interactions were detected for the last C-terminal residues, H11–R12 on YR-11 and L10–I11–R12 on OP3-4 (Fig. 11). These results are similar to that obtained for peptide-2 (R90–K99), which presented no interactions involving residues H100 and R101. Additionally, no energy contribution was attributed by quantum calculations to residue K10 from YR-11. Based on this, we can conclude that the proposed peptides are too long, each presenting three extra C-terminal residues that do not participate in the binding to RANKL and may disturb the peptide stability after binding, especially when long side chains are present (as in C-terminal R12).

Quantum calculations also revealed similar total binding energies for both peptides, YR-11 (-53.9 kcal mol^{-1} with $\varepsilon = 10$) and OP3-4 (-57.4 kcal mol^{-1} with $\varepsilon = 10$), which is in agreement with their equivalent inhibitory potential (around 90%). Interestingly, the average energetic contribution of the tripeptide core, I4–E5–F6, is very similar (-63.0 and -64.8 kcal mol^{-1} for YR-11 and OP3-4, respectively, with $\varepsilon = 10$), although it presents a higher value for E5 on OP3-4, and higher values for I4 and F6 on YR-11 (Fig. 11). In both cases, the binding energy presented by this tripeptide core is higher (more attractive) than the binding energy of the whole peptide. In fact, most of the remaining residues present less significant contributions, except for E93 (corresponding to E93 in OPG), which presents a high repulsive energy (17.5 and 19.0 kcal mol^{-1} for YR-11 and OP3-4, respectively, with $\varepsilon = 10$), offering little benefit or even disturbing peptide binding (Fig. 11). Since the dissociation rate of mimetics has been shown to correlate with biological activity, the presence of these extra amino acid residues may impact the efficiency of these peptides as therapeutic agents.[85] Based on this, our results emphasize that the key to osteoclastogenesis inhibition relies on the tripeptide core, I94–E95–F96, which is available as a template for designing small peptides with potential for the treatment of osteopenias.

4. Conclusions

The current analysis outlines a detailed energetic description of all the PPIs involved in the establishment of the RANKL–OPG complex, deepening our knowledge about osteoclastogenesis inhibition and highlighting the tripeptide core, I94–E95–F96, as the key for OPG functionality. Moreover, our results have provided a structural and energetic basis for Paget's disease and for the effective inhibition of RANKL by two previously described peptides.

We have considered water molecules in two different ways (treatments one and two) during the calculations, also applying two different values of the dielectric constant ($\varepsilon = 10$ and $\varepsilon = 40$), with the aim of properly analyzing the influence of the solvent over the binding energies. Our results indicate that both treatments are suitable for considering water molecules in the calculations, although the majority of analysed residues display an increased total binding energy for treatment two, pointing to a contributive role of water molecules over protein binding. Furthermore, lower values of the dielectric constant (around $\varepsilon = 10$) have proven appropriate to estimate important polar interactions without underestimating hydrophobic contacts.

Quantum calculations have confirmed the importance of site II for OPG binding and activity, mainly through the coordination

of interactions performed by the tripeptide core, I94–E95–F96. This tripeptide coordinates more than a half of all interactions involved in site II, contributing 53% of the total binding energy in the complex. The disruption of these interactions may lead to a severe impact on OPG functionality, such as that observed in Paget's disease. Our results have proven that the single mutation responsible for this autosomal recessive disease (F96L) generates a mutant OPG that is unable to properly bind RANKL due to a lack of stabilizing interactions. This fact emphasizes the crucial role of this tripeptide core, which is also the key to the high efficiency of the analysed inhibitory peptides, YR-11 and OP3-4, as attested by the structural and energy analyses. These assumptions corroborate the previous statement that OPG exerts its decoy receptor function by directly occupying binding site II and blocking the accessibilities of key interacting residues, such as R223 and K257, on RANKL, preventing RANK recognition.[10]

Nevertheless, it is important to highlight that, despite presenting a secondary role, site I stabilizes OPG along RANKL's surface, allowing precise insertion of the 90s loop into binding site II. Previous results have indicated that mutations affecting OPG's residues on binding site I had almost no impact over the complex formation, but we have attested through quantum calculations a collaborative association of several minor interactions at this site.[10] This result indicates peptide-1 as a potential template for the design of inhibitory molecules targeting a broader spot on RANKL.

Currently, the design of inhibitory peptides targeting the RANK–RANKL–OPG molecular triad is based solely on the structural analysis of crystal structures, validated by biological assays. Some of the proposed peptides have proven useful and able to efficiently inhibit osteoclastogenesis. Nevertheless, our quantum calculations indicate that the inhibitory potential of these peptides relies on the tripeptide core, I–E–F, attributing to the remaining residues a minor role (or even a disturbing role) over the process. Based on this, we propose the design of small and specific peptides based on this tripeptide core as an innovative strategy for RANK–RANKL complex inhibition. These peptides would present better stability, specificity and cost, emerging as important tools for the treatment of osteoporosis and other osteopenias.

Acknowledgements

This study was partially supported by Fundação de Amparo à Pesquisa do Estado de Minas Gerais (PRONEX/FAPEMIG-Brazil), Conselho Nacional de Desenvolvimento Científico e Tecnológico (CNPq), and Coordenação de Aperfeiçoamento de Pessoal de Nível Superior (CAPES).

References

1 T. J. Martin and N. A. Sims, *Trends Mol. Med.*, 2005, **11**, 76–81.
2 J. C. Crockett, M. J. Rogers, F. P. Coxon, L. J. Hocking and M. H. Helfrich, *J. Cell Sci.*, 2011, **124**, 991–998.
3 N. A. Sims and J. H. Gooi, *Semin. Cell Dev. Biol.*, 2008, **19**, 444–451.
4 B. F. Boyce and L. Xing, *Arthritis Res. Ther.*, 2007, **9**, S1.
5 D. L. Lacey, W. J. Boyle, W. S. Simonet, P. J. Kostenuik, W. C. Dougall, J. K. Sullivan, J. S. Martin and R. Dansey, *Nat. Rev. Drug Discovery*, 2012, **11**, 401–419.
6 D. M. Anderson, E. Maraskovsky, W. L. Billingsley, W. C. Dougall, M. E. Tometsko, E. R. Roux, M. C. Teepe, R. F. DuBose, D. Cosman and L. Galibert, *Nature*, 1997, **390**, 175–179.
7 B. R. Wong, J. Rho, J. Arron, E. Robinson, J. Orlinick, M. Chao, S. Kalachikov, E. Cayani, F. S. Bartlett, W. N. Frankel, S. Y. Lee and Y. Choi, *J. Biol. Chem.*, 1997, **272**, 25190–25194.
8 A. Hikita, I. Yana, H. Wakeyama, M. Nakamura, Y. Kadono, Y. Oshima, K. Nakamura, M. Seiki and S. Tanaka, *J. Biol. Chem.*, 2006, **281**, 36846–36855.
9 H. Yasuda, N. Shima, N. Nakagawa, K. Yamaguchi, M. Kinosaki, S. Mochizuki, A. Tomoyasu, K. Yano, M. Goto, A. Murakami, E. Tsuda, T. Morinaga, K. Higashio, N. Udagawa, N. Takahashi and T. Suda, *Proc. Natl. Acad. Sci. U. S. A.*, 1998, **95**, 3597–3602.
10 X. Luan, Q. Lu, Y. Jiang, S. Zhang, Q. Wang, H. Yuan, W. Zhao, J. Wang and X. Wang, *J. Immunol.*, 2012, **189**, 245–252.
11 J. Luo, Z. Yang, Y. Ma, Z. Yue, H. Lin, G. Qu, J. Huang, W. Dai, C. Li, C. Zheng, L. Xu, H. Chen, J. Wang, D. Li, S. Siwko, J. M. Penninger, G. Ning, J. Xiao and M. Liu, *Nat. Med.*, 2016, **22**, 539–546.
12 C. V. Gurban and O. Mederle, *Rom. J. Morphol. Embryol.*, 2012, **52**, 1113–1119.
13 N. Bucay, I. Sarosi, C. R. Dunstan, S. Morony, J. Tarpley, C. Capparelli, S. Scully, H. L. Tan, W. Xu, D. L. Lacey, W. J. Boyle and W. S. Simonet, *Genes Dev.*, 1998, **12**, 1260–1268.
14 A. Leibbrandt and J. M. Penninger, *Ann. N. Y. Acad. Sci.*, 2008, **1143**, 123–150.
15 Y. Y. Kong, H. Yoshida, I. Sarosi, H. L. Tan, E. Timms, C. Capparelli, S. Morony, A. J. Oliveira-dos-Santos, G. Van, A. Itie, W. Khoo, A. Wakeham, C. R. Dunstan, D. L. Lacey, T. W. Mak, W. J. Boyle and J. M. Penninger, *Nature*, 1999, **397**, 315–323.
16 S. W. Rossi, M.-Y. Kim, A. Leibbrandt, S. M. Parnell, W. E. Jenkinson, S. H. Glanville, F. M. McConnell, H. S. Scott, J. M. Penninger, E. J. Jenkinson, P. J. L. Lane and G. Anderson, *J. Exp. Med.*, 2007, **204**, 1267–1272.
17 H. Takayanagi, *Nat. Rev. Immunol.*, 2007, **7**, 292–304.
18 M. N. Weitzmann, *Scientifica*, 2013, **2013**, 125705.
19 J. E. Fata, Y. Y. Kong, J. Li, T. Sasaki, J. Irie-Sasaki, R. A. Moorehead, R. Elliott, S. Scully, E. B. Voura, D. L. Lacey, W. J. Boyle, R. Khokha and J. M. Penninger, *Cell*, 2000, **103**, 41–50.
20 R. Hanada, A. Leibbrandt, T. Hanada, S. Kitaoka, T. Furuyashiki, H. Fujihara, J. Trichereau, M. Paolino, F. Qadri, R. Plehm, S. Klaere, V. Komnenovic, H. Mimata, H. Yoshimatsu, N. Takahashi, A. von Haeseler, M. Bader, S. S. Kilic, Y. Ueta, C. Pifl, S. Narumiya and J. M. Penninger, *Nature*, 2009, **462**, 505–509.

21 A. H. Mohammadpour, J. Shamsara, S. Nazemi, S. Ghadirzadeh, S. Shahsavand and M. Ramezani, *Thrombosis*, 2012, **2012**, 306263.
22 D. H. Jones, T. Nakashima, O. H. Sanchez, I. Kozieradzki, S. V. Komarova, I. Sarosi, S. Morony, E. Rubin, R. Sarao, C. V. Hojilla, V. Komnenovic, Y.-Y. Kong, M. Schreiber, S. J. Dixon, S. M. Sims, R. Khokha, T. Wada and J. M. Penninger, *Nature*, 2006, **440**, 692–696.
23 C. H. Siar, H. Tsujigiwa, I. Ishak, N. M. Hussin, H. Nagatsuka and K. H. Ng, *J. Oral Med. Oral Surg. Oral Pathol. Oral Radiol.*, 2015, **119**, 83–91.
24 D. Schramek, A. Leibbrandt, V. Sigl, L. Kenner, J. A. Pospisilik, H. J. Lee, R. Hanada, P. A. Joshi, A. Aliprantis, L. Glimcher, M. Pasparakis, R. Khokha, C. J. Ormandy, M. Widschwendter, G. Schett and J. M. Penninger, *Nature*, 2010, **468**, 98–102.
25 B. Ma, Q. Zhang, D. Wu, Y. Wang, Y. Hu, Y. Cheng, Z. Yang, Y. Zheng and H.-J. Ying, *Acta Pharmacol. Sin.*, 2012, **33**, 479–489.
26 K. Redlich and J. S. Smolen, *Nat. Rev. Drug Discovery*, 2012, **11**, 234–250.
27 S. Khosla, *J. Gerontol., Ser. A*, 2013, **68**, 1226–1235.
28 M. V. Clarke, P. K. Russell, D. M. Findlay, S. Sastra, P. H. Anderson, J. P. Skinner, G. J. Atkins, J. D. Zajac and R. A. Davey, *Endocrinology*, 2015, **156**, 3203–3214.
29 Q. Rehman and N. E. Lane, *Arthritis Res.*, 2001, **3**, 221–227.
30 D. Heymann, *J. Bone Oncol.*, 2012, **1**, 2–11.
31 W. Takasaki, Y. Kajino, K. Kajino, R. Murali and M. Greene, *Nat. Biotechnol.*, 1997, **15**, 1266–1270.
32 T. Wada, T. Nakashima, N. Hiroshi and J. M. Penninger, *Trends Mol. Med.*, 2006, **12**, 17–25.
33 J. P. Xie, M. Namjoshi, E. Q. Wu, K. Parikh, M. Diener, A. P. Yu, A. Guo and K. W. Culver, *J. Manag. Care Pharm.*, 2011, **17**, 621.
34 E. S. Orwoll, W. H. Scheele, S. Paul, S. Adami, U. Syversen, A. Diez Perez, J. M. Kaufman, A. D. Clancy, G. A. Gaich, A. Diez-Perez, J. M. Kaufman, A. D. Clancy and G. A. Gaich, *J. Bone Miner. Res.*, 2003, **18**, 9–17.
35 E. S. Orwoll, J. Shapiro, S. Veith, Y. Wang, J. Lapidus, C. Vanek, J. L. Reeder, T. M. Keaveny, D. C. Lee, M. A. Mullins, S. C. S. Nagamani and B. Lee, *J. Clin. Invest.*, 2014, **124**, 491–498.
36 V. Subbiah, V. S. Madsen, A. K. Raymond, R. S. Benjamin and J. A. Ludwig, *Osteoporosis Int.*, 2010, **21**, 1041–1045.
37 L. G. Milroy, T. N. Grossmann, S. Hennig, L. Brunsveld and C. Ottmann, *Chem. Rev.*, 2014, **114**, 4695–4748.
38 M. Pelay-Gimeno, A. Glas, O. Koch and T. N. Grossmann, *Angew. Chem., Int. Ed.*, 2015, **54**, 2–34.
39 K. Fosgerau and T. Hoffmann, *Drug Discovery Today*, 2015, **20**, 122–128.
40 V. J. Hruby and M. Cai, *Annu. Rev. Pharmacol. Toxicol.*, 2013, **53**, 557–580.
41 D. J. Craik, D. P. Fairlie, S. Liras and D. Price, *Chem. Biol. Drug Des.*, 2013, **81**, 136–147.
42 P. Vlieghe, V. Lisowski, J. Martinez and M. Khrestchatisky, *Drug Discovery Today*, 2010, **15**, 40–56.
43 N. London, D. Movshovitz-Attias and O. Schueler-Furman, *Structure*, 2010, **18**, 188–199.
44 P. Rezácová, D. Borek, S. F. Moy, A. Joachimiak and Z. Otwinowski, *Proteins*, 2008, **70**, 311–319.
45 T. Geppert, B. Hoy, S. Wessler and G. Schneider, *Chem. Biol.*, 2011, **18**, 344–353.
46 C. Liu, Y. Zhao, W. He, W. Wang, Y. Chen, S. Zhang, Y. Ma, J. Gohda, T. Ishida, T. S. Walter, R. J. Owens, D. I. Stuart, J. Ren and B. Gao, *Sci. Rep.*, 2015, **5**, 14150.
47 C. A. Nelson, J. T. Warren, M. W.-H. Wang, S. L. Teitelbaum and D. H. Fremont, *Structure*, 2012, **20**, 1971–1982.
48 L. A. Schneeweis, D. Willard and M. E. Milla, *J. Biol. Chem.*, 2005, **280**, 41155–41164.
49 S. Tanaka, K. Nakamura, N. Takahasi and T. Suda, *Immunol. Rev.*, 2005, **208**, 30–49.
50 T. Zhou, D. Z. Huang and A. Caflisch, *Curr. Top. Med. Chem.*, 2010, **10**, 33–45.
51 M. W. Van Der Kamp and A. J. Mulholland, *Biochemistry*, 2013, **52**, 2708–2728.
52 A. Monari, J. L. Rivail and X. Assfeld, *Acc. Chem. Res.*, 2013, **46**, 596–603.
53 E. L. Wu, Y. Mei, K. Han and J. Z. H. Zhang, *Biophys. J.*, 2007, **92**, 4244–4253.
54 P. Hohenberg and W. Kohn, *Phys. Rev.*, 1964, **136**, B864–B871.
55 W. Kohn and L. J. Sham, *Phys. Rev.*, 1965, **140**, A1133–A1138.
56 W. L. Jorgensen, *Science*, 2004, **303**, 1813–1818.
57 J. Hafner, *Nat. Mater.*, 2010, **9**, 690–692.
58 X. Chen, Y. Zhang and J. Z. H. Zhang, *J. Chem. Phys.*, 2005, **122**, 184105.
59 X. He and K. M. Merz Jr, *J. Chem. Theory Comput.*, 2010, **6**, 405–411.
60 M. S. Gordon, D. G. Fedorov, S. R. Pruitt and L. V Slipchenko, *Chem. Rev.*, 2012, **112**, 632–672.
61 I. L. Barroso-Neto, J. P. C. Marques, R. F. Costa, E. W. S. Caetano, B. S. Cavada, C. Gottfried and V. N. Freire, *J. Phys. Chem. B*, 2012, **116**, 3270–3279.
62 R. F. Costa, V. N. Freire, E. M. Bezerra, B. S. Cavada, E. W. S. Caetano, J. L. Lima Filho and E. L. Albuquerque, *Phys. Chem. Chem. Phys.*, 2012, **14**, 1389–1398.
63 G. Zanatta, I. L. Barroso-Neto, M. F. D. Victorio Bambini-Junior, E. M. Bezerra, R. F. Costa, E. W. S. Caetano, B. S. Cavada, V. N. Freire and C. Gottfried, *J. Proteomics Bioinf.*, 2012, **05**, 155–162.
64 G. Zanatta, G. Nunes, E. M. Bezerra, R. F. Costa, A. Martins, E. W. S. Caetano, V. N. Freire and C. Gottfried, *ACS Chem. Neurosci.*, 2014, **5**, 1041–1054.
65 A. C. V. Martins, P. de Lima-Neto, I. L. Barroso-Neto, B. S. Cavada, V. N. Freire and E. W. S. Caetano, *RSC Adv.*, 2013, **3**, 14988.
66 J. X. Lima Neto, U. L. Fulco, E. L. Albuquerque, G. Corso, E. M. Bezerra, E. W. S. Caetano, R. F. Costa and V. N. Freire, *Phys. Chem. Chem. Phys.*, 2015, **17**, 13092–13103.
67 T. C. Silva Ribeiro, R. F. Costa, E. M. Bezerra, V. N. Freire, M. L. Lyra and V. Manzoni, *New J. Chem.*, 2014, **38**, 2946.

68 D. S. Dantas, J. I. N. Oliveira, J. X. Lima Neto, R. F. Costa, E. M. Bezerra, V. N. Freire, E. W. S. Caetano, U. L. Fulco and E. L. Albuquerque, *RSC Adv.*, 2015, **5**, 49439–49450.
69 C. R. F. Rodrigues, J. I. N. Oliveira, U. L. Fulco, E. L. Albuquerque, R. M. Moura, E. W. S. Caetano and V. N. Freire, *Chem. Phys. Lett.*, 2013, **559**, 88–93.
70 A. Warshel, P. K. Sharma, M. Kato and W. W. Parson, *Biochim. Biophys. Acta*, 2006, **1764**, 1647–1676.
71 C. N. Schutz and A. Warshel, *Proteins: Struct., Funct., Genet.*, 2001, **417**, 400–417.
72 G. N. Patargias, S. A. Harris and J. H. Harding, *J. Chem. Phys.*, 2010, **132**, 235103.
73 J. C. Phillips, R. Braun, W. Wang, J. Gumbart, E. Tajkhorshid, E. Villa, C. Chipot, R. D. Skeel, L. Kalé and K. Schulten, *J. Comput. Chem.*, 2005, **26**, 1781–1802.
74 B. Delley, *J. Chem. Phys.*, 2000, **113**, 7756–7764.
75 A. Tkatchenko, R. A. Distasio, R. Car and M. Scheffler, *Phys. Rev. Lett.*, 2012, **236402**, 1–5.
76 D. W. Zhang and J. Z. H. Zhang, *J. Chem. Phys.*, 2003, **119**, 3599.
77 R. A. Engh and R. Huber, *Acta Crystallogr., Sect. A: Found. Crystallogr.*, 1991, **47**, 392–400.
78 A. Klamt and G. Schuurmann, *J. Chem. Soc., Perkin Trans. 2*, 1993, 799–805.
79 S. Vicatos, M. Roca and A. Warshel, *Proteins: Struct., Funct., Bioinf.*, 2009, **77**, 670–684.
80 J. Antony and S. Grimme, *J. Comput. Chem.*, 2012, **33**, 1730–1739.
81 A. Warshel, S. T. Russell and A. K. Churg, *Proc. Natl. Acad. Sci. U. S. A.*, 1984, **81**, 4785–4789.
82 A. C. V Martins, F. W. P. Ribeiro, G. Zanatta, V. N. Freire, S. Morais, P. Lima-Neto and A. N. Correia, *Bioelectrochemistry*, 2016, **108**, 46–53.
83 W. Humphrey, A. Dalke and K. Schulten, *J. Mol. Graphics*, 1996, **14**, 33–38.
84 V. G. M. Naidu, K. R. Dinesh Babu, M. M. Thwin, R. L. Satish, P. V. Kumar and P. Gopalakrishnakone, *Chem.-Biol. Interact.*, 2013, **203**, 467–479.
85 X. Cheng, M. Kinosaki, M. Takami, Y. Choi, H. Zhang and R. Murali, *J. Biol. Chem.*, 2004, **279**, 8269–8277.
86 O. Trott and A. J. Olson, *J. Comput. Chem.*, 2009, **31**, 455–651.
87 A. K. Rajagopal and J. Callaway, *Phys. Rev. B: Solid State*, 1973, **7**, 1912–1919.
88 S. Téletchéa, V. Stresing, S. Hervouet, M. Baud'huin, M. F. Heymann, G. Bertho, C. Charrier, K. Ando and D. Heymann, *J. Bone Miner. Res.*, 2014, **29**, 1466–1477.
89 C. Liu, T. S. Walter, P. Huang, S. Zhang, X. Zhu, Y. Wu, L. R. Wedderburn, P. Tang, R. J. Owens, D. I. Stuart, J. Ren and B. Gao, *J. Immunol.*, 2010, **184**, 6910–6919.
90 G. Roodman and J. Windle, *J. Clin. Invest.*, 2005, **115**, 200–207.
91 W. Wuyts, L. Van Wesenbeeck, A. Morales-Piga, S. Ralston, L. Hocking, F. Vanhoenacker, R. Westhovens, L. Verbruggen, D. Anderson, A. Hughes and W. Van Hul, *Bone*, 2001, **28**, 104–107.